Self-Tuned Quantum Dot Gain in Photonic Crystal Lasers

S. Strauf,[1,2,*] K. Hennessy,[3] M. T. Rakher,[2] Y.-S. Choi,[3] A. Badolato,[3] L. C. Andreani,[4] E. L. Hu,[1,3] P. M. Petroff,[1,3] and D. Bouwmeester[2]

[1]*Materials Department, University of California Santa Barbara, Santa Barbara, California 93106, USA*
[2]*Department of Physics, University of California Santa Barbara, Santa Barbara, California 93106, USA*
[3]*ECE Department, University of California Santa Barbara, Santa Barbara, California 93106, USA*
[4]*Department of Physics "A. Volta," University of Pavia, 27100 Pavia, Italy*

(Received 20 November 2005; published 31 March 2006)

We demonstrate that very few (2–4) quantum dots as a gain medium are sufficient to realize a photonic-crystal laser based on a high-quality nanocavity. Photon correlation measurements show a transition from a thermal to a coherent light state proving that lasing action occurs at ultralow thresholds. Observation of lasing is unexpected since the cavity mode is in general not resonant with the discrete quantum dot states and emission at those frequencies is suppressed. In this situation, the quasicontinuous quantum dot states become crucial since they provide an energy-transfer channel into the lasing mode, effectively leading to a *self-tuned* resonance for the gain medium.

DOI: 10.1103/PhysRevLett.96.127404 PACS numbers: 78.67.Hc, 42.50.Ar, 42.55.Tv, 78.55.Cr

Optical microcavities [1], in particular, photonic-crystal membranes, offer the ability to create new, efficient optical sources of specified wavelength through the control of the dielectric environment. Extremely low-threshold lasers can result from the appropriate match of small mode-volume photonic-crystal cavities to optically active material. One measure of the optical efficiency of a laser is the spontaneous emission (SE) coupling factor β. The theoretical limit is one, corresponding to the hypothetical case of thresholdless lasing. Microdisk [2,3] and photonic-crystal lasers (PCL) [4] with quantum wells (QW) or a high density of quantum dots (QD) as the medium show values ranging from 0.1 to 0.2, but a pronounced lasing threshold behavior remains [2–7]. For nonlasing devices β values above 0.9 have been estimated [8]. Here we report on PCLs sustained by only 2–4 QDs as the active gain material showing ultralow lasing thresholds and a β of 0.85.

To achieve lasing operation, both the gain medium and the cavity must have exceptional features. The cavity design shown in Fig. 1(a) is based on a line defect of three missing air holes ($L3$ type) within a triangular lattice formed in a 126 nm GaAs membrane, acting as a monomode waveguide in the QD emission range. The center of the membrane contains a single layer of low-density ($8 \pm 2\ \mu\mathrm{m}^{-2}$) InAs QDs grown by the partially covered island technique [9]. This leads to QDs with shallow confinement energies and a pronounced density of extended wetting layer (WL) states [10]. Neighboring holes in the line have been shifted outwards [as indicated by white arrows in Fig. 1(a)] to produce better confinement of the mode [11]. To achieve optimal coupling of the lasing mode with the active QD gain material, two new design concepts have been employed. First, the two holes nearest to the defect have been reduced by 20% in size to decrease their overlap with high field regions [12]. Second, the width w of the channel region containing the three missing holes has been increased by 30 nm, as illustrated by the gray shading in Fig. 1(a). In culmination, these design concepts achieve a mode volume of $V = 0.68(\lambda/n)^3$ and an effective refractive index n_{eff} of 2.9, a very high value for this class of porous cavity membranes. In addition, this design ensures that the field maximum is in excellent spatial overlap with the gain medium while the overlap with the air-semiconductor interface is drastically reduced. Such interfaces are detrimental since the optical properties of QDs

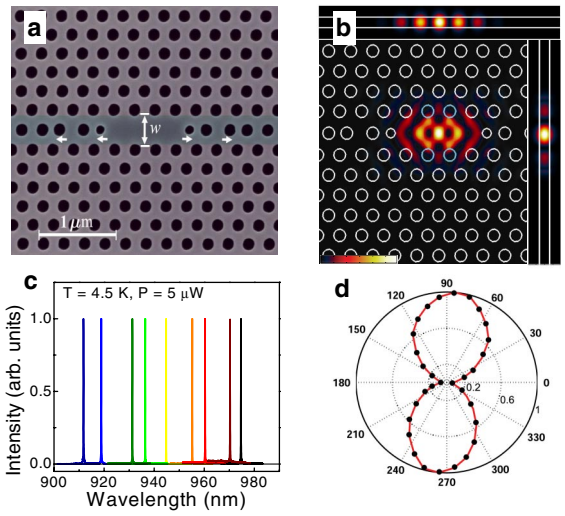

FIG. 1 (color online). (a) Scanning electron micrograph around the defect region of a PCL laser with a lattice constant of 260 nm. (b) Plot of the electric field intensity of the lasing mode as calculated from 3D finite-difference time-domain simulations [23]. (c) Normalized lasing mode spectra for 9 different PCL devices taken at a pump power of 5 μW, $T = 4.5$ K. (d) Measured cavity mode intensity as a function of polarizer angle showing a polarization ratio of 25:1.

near surfaces degrade critically [13], and surface defect states can be optically absorbing.

The wavelength of the PCL mode can be tuned through its lattice parameters to the SE wavelength range of the QD gain medium. We studied 22 PCL devices ranging from 908 to 975 nm covering the ground state (s shell, centered at 965 nm) and excited state (p shell) of the embedded QDs. The QDs were excited via the GaAs matrix by a continuous wave (cw) 780 nm laser diode using a microscope objective. The effective spot size including carrier diffusion was estimated from lateral scanning of the single QD emission to be 3.4 μm. Despite the fact that there are on average only 2 to 4 QDs located within the mode volume and that the exciton transitions of those QDs are in general off resonance with the cavity mode, we claim that most devices show pronounced single-mode lasing [Figs. 1(c) and 1(d)].

Before discussing the remarkable laser gain process, we present three different experimental evidences for lasing operation. First, we recorded the output power of the cavity mode as a function of cw-excitation pump power. Figure 2(a) shows the resulting L-L curve for a device emitting at 960 nm (solid dots). Above a certain threshold pump power, a linear increase in output intensity is observed, as indicated by the red line. The conventional estimation of the cw lasing threshold, obtained by extrapolation of the red line to zero output power [Fig. 2(b)], yields a value of 124 nW (1.3 W/cm^2), corresponding to an absorbed pump power of only 4 nW (49 mW/cm^2). This is an improvement of 2 to 3 orders of magnitude over prior reports [1–7]. We measured similar ultralow threshold values for temperatures between 4 and 80 K. For higher temperatures the QD emission is quenched due to the thermal breakup of excitons. Figure 2(b) shows no sharp threshold but a soft turn-on of the cavity mode intensity, in accordance with theory for a large SE coupling efficiency [14,15].

A second characteristic of a laser is the emission linewidth narrowing profile. Below and above threshold the linewidth ΔE varies inversely with the output power [16]. At threshold, the phase transition into lasing leads to a pronounced kink in the profile [17], as demonstrated in Fig. 3(a). To compare the linewidth narrowing with the intensity data [Fig. 3(b)] the linewidth is plotted as a function of pump power. In principal, a contribution to linewidth narrowing could also arise from loss saturation effects of QDs. These effects, however, do not lead to a kink in the L-L curve, as has been confirmed by additional measurements performed on nonlasing devices. Those measurements follow the dotted blue lines in Fig. 3. Such behavior corresponds to operation in the light-emitting-diode (LED) regime and is similar to the standard Schawlow-Townes linewidth narrowing below threshold, where there is a constant cavity loss but an increase in gain [16]. We found that maximum output powers for devices operating in the LED regime are an order of magnitude lower compared to those reaching the lasing regime. For the best lasing devices the $E/\Delta E$ ratios reach values up to 32 000 and the corresponding Q factors measured at pump powers below lasing threshold range between 7800 and 18 000.

To provide a third and direct proof that lasing action occurs, we measured the second order photon correlation function $g^2(\tau) = \langle I(t)I(t+\tau)\rangle/\langle I(t)\rangle\langle I(t)\rangle$, where $\langle I(t)\rangle$ is the expectation value of the intensity in the cavity mode at time t, as a function of excitation pump power [Fig. 2(c)]. The cavity mode emission was spectrally filtered with a 0.5 nm bandpass and sent to a Hanbury Brown–Twiss (HBT) interferometer, consisting of a 50/50 beam splitter and two single photon counting detectors, as shown schematically in the inset of Fig. 2(c). Photon coincidences were recorded electronically as a histogram of start-stop

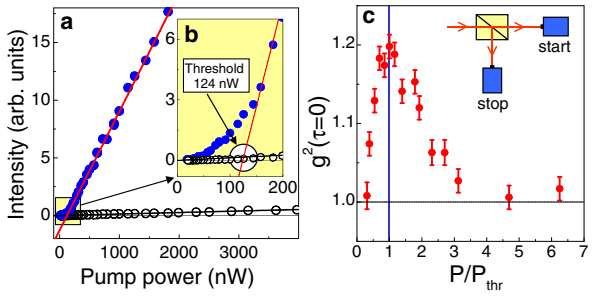

FIG. 2 (color online). (a) Lasing mode intensity (solid dots) and SE background (open dots) as a function of excitation pump power for a cavity emitting at 960 nm. Red line: linear fit. (b) Magnification of threshold region. (c) Photon correlation function $g^2(\tau = 0)$ of the cavity mode as a function of normalized pump power P/P_{thr}. Absorbed pump power at threshold, P_{thr}, for this device emitting at 940 nm is 25 nW. $T = 4.5$ K.

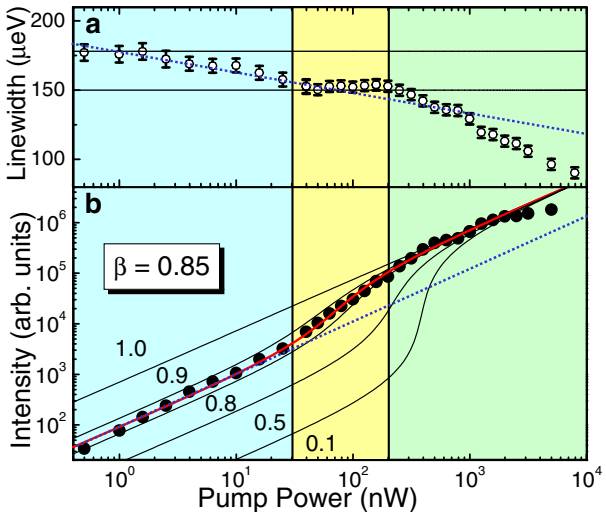

FIG. 3 (color online). Cavity mode linewidth (a) and intensity (b) as a function of excitation pump power (solid dots). The x axis displays optical power sent into the cavity. The corresponding absorbed pump powers are 3.6% of these values. Solid lines: Rate equation model solutions for various values of β. Red line: Best fit corresponding to $\beta = 0.85 \pm 0.03$. Dotted blue lines indicate the measured behavior for nonlasing devices.

events. A characteristic feature of a laser is the phase transition from a thermal into a coherent light state as a function of pump rate [18]. The measured photon bunching signature $[g^2(\tau = 0) > g^2(\tau)]$ around the threshold of the PCL indicates the thermal character of the emitted light field. Below threshold $g^2(\tau = 0)$ should theoretically approach a value of two corresponding to an ideal thermal state. However, the measured values for $g^2(\tau = 0)$ drop down at lowest pump powers due to a decrease of the coherence length of the PCL emission approaching the temporal resolution limit (450 ps) of the HBT setup [19]. At pump powers above threshold the cavity mode picks up phase coherence due to stimulated emission, leading to a transition into a coherent light state where $g^2(\tau = 0)$ approaches unity [Fig. 2(c)]. In addition, we performed experiments on a series of photonic-crystal cavities designed to span the range from $\beta = 0.3$ to $\beta = 0.9$ as well as on a commercial semiconductor laser diode confirming that Fig. 2(c) is indeed characteristic for lasing action [19].

To extract the fraction β of SE into the lasing mode with respect to SE into all available modes, we use a coupled rate equation model for the carrier density N and the photon density P of a semiconductor laser diode [16]:

$$\frac{dN}{dt} = R_p - \frac{N}{\tau_{\mathrm{sp}}} - \frac{N}{\tau_{\mathrm{nr}}} - v_g g P, \tag{1}$$

$$\frac{dP}{dt} = v_g \Gamma g P + \Gamma \beta \frac{N}{\tau_{\mathrm{sp}}} - \frac{P}{t_c}, \tag{2}$$

where R_p is the pump rate, v_g the group velocity, Γ the confinement factor, $1/t_c$ the cavity photon loss rate, $1/t_{\mathrm{sp}}$ the spontaneous, and $1/t_{\mathrm{nr}}$ the nonradiative recombination rate. Steady state solutions have been found assuming a linear gain function $g = a(N - N_{\mathrm{tr}})$, where a is the differential gain and N_{tr} the transparency carrier density. The solid lines shown in Fig. 3(b) are solutions of the rate equations for various values of β keeping all other parameters constant. Parameters used are determined as follows: A t_c of 4.1 ps corresponds to the measured $Q = 9800$. Lifetime measurements at the cavity mode frequency reveal $t_{\mathrm{sp}} = 0.14$ ns. The t_{nr} has been taken to be 10 ns and does not influence the fit considerably [14]. A Γ of 0.004 has been estimated from the intersection of the mode volume with the single layer of QDs and $v_g = c/n_{\mathrm{eff}} = 1 \times 10^{10}$ cm/s. Best fits have been found for $a = 4.5 \times 10^{-10}$ cm^2 and $N_{\mathrm{tr}} = 5.5 \times 10^{14}$ cm^{-3}. The corresponding material gain of 2×10^5 cm^{-1} is in good agreement with values for other InAs QD lasers [20]. The transparency (threshold) carrier density corresponds to about 8 (18) electron hole pairs within the mode volume. The red curve in Fig. 3(b) is the best fit for $\beta = 0.85 \pm 0.03$ which implies an ultrahigh SE coupling efficiency of 85%. Note that the nonlinear kink in the intensity data occurs at the same pump power values as the kink in the linewidth narrowing [Fig. 3(a)] and the soft turn-on starting at about 30 nW incident pump power corresponds to the definition of the lasing threshold for high-β lasers [14].

In general, the β factor depends on the number of optical modes and the width of the SE spectrum. Besides the fundamental cavity mode, the density of radiation modes is strongly suppressed. This is supported by measured lifetimes up to 10 ns for single QDs located outside of the cavity mode region but within the photonic-crystal membrane. These values are 1 order of magnitude larger than SE lifetimes (1 ns) measured in unprocessed areas of the wafer. The observed inhibition directly reflects the low density of radiation modes within the photonic bandgap. It has been predicted that nondegenerate fundamental modes in PCL structures with similar mode profiles can achieve β values up to 0.87 assuming a SE bandwidth of 25 nm [21]. While such a bandwidth can be achieved with QWs or larger ensembles of QDs [7], it is indeed very surprising that at our low QD densities such an efficient QD-cavity coupling occurs. The sharp exciton QD emission wavelength is statistically distributed over 50 nm making a simultaneous spectral and spatial coupling very unlikely ($<1\%$). Control samples containing zero QDs but a dominant WL emission at 860 nm do not show lasing or any decoration of the cavity mode. If there is only one QD spatially overlapping with the cavity mode, as has been confirmed by deterministic QD positioning [22], decoration of the mode occurs even for up to 20 nm spectral detuning [23]. Therefore, the quantum dot cavity interaction has to involve an indirect and novel process.

To obtain insight into the underlying gain mechanism, we studied the spectral properties of a single QD located in an unprocessed area of the wafer [Figs. 4(a) and 4(b)]. The sharp transitions of the s shell emission evolve with increasing pump power into spectrally broad bands [Fig. 4(a) top]. This broad background is significant at pump powers around the lasing threshold [Fig. 4(b)] and demonstrates that SE from a single QD occurs over a large frequency range. Several effects are responsible for the rich spectral properties. Multiple charge states of the exciton (X^+, X^0, X^-) [24] and biexcitons (XX) [25] give rise to a few recombination lines. Each transition deviates from a Lorentzian line shape in the form of a broad background extending about 4 meV (not shown) due to electron-acoustic phonon coupling [26]. It is furthermore known that in these QDs with shallow confinement, the transitions between localized QD states and extended WL states provide a quasicontinuum covering the energy region between the WL and the p shell [10], as has been indicated by regions I and II in Fig. 4(c), respectively. At pump powers around the lasing threshold, these states are already appreciably populated. In this case, when multiexciton states are involved, the recombination energy of the s shell strongly depends on the exact exciton number and spin configuration in the p shell [27] and extended states. Therefore, this intradot Coulomb interaction produces a configuration mixing between s and p shells and couples the extended state continuum around the p shell into the energy region

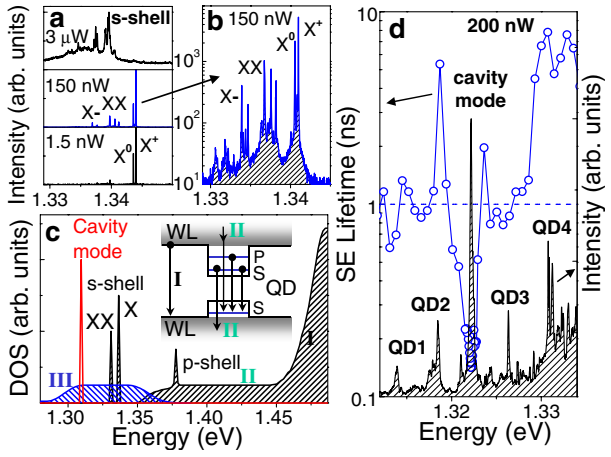

FIG. 4 (color online). (a) Single QD spectra recorded at pump powers below (1.5 nW), around (150 nW) and above (1.5 μW) the lasing threshold of the PCLs. (b) 150 nW spectrum on a log scale illustrating the broad background. (c) Schematic illustration of the possible in-plane transitions of a single QD adjacent to a WL (inset) and the corresponding density of states (DOS). (d) PCL spectrum taken at 200 nW (right y axis) and measured SE lifetimes as a function of energy using a 0.1 meV broad spectral window (left y axis). Sharp lines right next to the cavity mode have been tentatively labeled by QD1-QD4.

of the s shell emission, thereby causing a broad emission background as shown in Fig. 4(a) (top) and indicated by region III in Fig. 4(c). The many-body coupling between s and p shells requires the Coulomb interaction to be included into the emission process, and in this sense it is different from a two-step, Auger-like relaxation process.

The essential role of the nanocavity, in contrast to a large cavity with many modes per unit frequency, is the strong inhibition of sharp exciton transitions up to 1 order of magnitude, as can be seen exemplarily for QD2 and QD4 in Fig. 4(d). Simultaneously, the combined QD-WL states become crucial since their energy resonance condition is easily fulfilled, leading to an effective transfer channel into the lasing mode. Measured SE lifetimes on top of the cavity mode are as fast as 145 ps [Fig. 4(d)]. Temperature tuning experiments revealed that none of the sharp QD transitions were in spectral resonance with the cavity mode. Note that not all of the QDs experience inhibition [see QD1 and QD3 in Fig. 4(d)]. This is expected since about 20% of QDs are close to surfaces that lead to additional nonradiative loss channels [13]. In culmination, the QD confinement potential harvests the excitons and their coupling to the surrounding matrix efficiently transfers the energy into the lasing mode.

In summary, we observe lasing action as demonstrated by the characteristic L-L curve, linewidth narrowing profile, and photon statistics. We have shown that lasing in single-mode photonic-crystal cavities does not require an exciton-mode resonance. These results challenge the conventional QD-laser design based on incorporating several dense layers of QD material. This has clear technological implications for the future design of ultraefficient nanoscale lasers, which may now be formed with only a few, or even single, QDs that, with cooperation from the surrounding matrix, *self-tune* their emission into the lasing mode with nearly perfect efficiency.

This research has been supported by DARPA Grant No. MDA972-01-1-0027 and NSF NIRT Grant No. 0304678.

*Corresponding author.
Electronic address: strauf@physics.ucsb.edu

[1] K. J. Vahala, Nature (London) **424**, 839 (2003).
[2] R. E. Slusher *et al.*, Appl. Phys. Lett. **63**, 1310 (1993).
[3] L. Z. Zhang and E. Hu, Appl. Phys. Lett. **82**, 319 (2003).
[4] H.-Y Ryu, M. Notomi, E. Kuramoti, and T. Segawa, Appl. Phys. Lett. **84**, 1067 (2004); H.-G. Park *et al.*, Science **305**, 1444 (2004).
[5] O. Painter *et al.*, Science **284**, 1819 (1999); T. Yoshie, O. B. Shchekin, H. Chen, D. G. Deppe, and A. Scherer, Electron. Lett. **38**, 967 (2002).
[6] M. Roehner, J. P. Reithmaier, A. Forchel, F. Schaefer, and H. Zull, Appl. Phys. Lett. **71**, 488 (1997).
[7] P. Michler *et al.*, Appl. Phys. Lett. **77**, 184 (2000).
[8] A. Kress *et al.*, Phys. Rev. B **71**, 241304 (2005).
[9] J. M. Garcia, P. Mankad, P. O. Holtz, P. J. Wellman, and P. M. Petroff, Appl. Phys. Lett. **72**, 3172 (1998).
[10] A. Vasanelli, R. Ferreira, and G. Bastard, Phys. Rev. Lett. **89**, 216804 (2002); B. Urbaszek *et al.*, Phys. Rev. B **69**, 035304 (2004).
[11] Y. Akahane, T. Asano, B.-S. Song, and S. Noda, Nature (London) **425**, 944 (2003); Opt. Express **13**, 1202 (2005).
[12] L. C. Andreani, D. Gerace, and M. Agio, Photon. Nanostruct. **2**, 103 (2004).
[13] C. F. Wang *et al.*, Appl. Phys. Lett. **85**, 3423 (2004).
[14] G. Björk, A. Karlsson, and Y. Yamamoto, Phys. Rev. A **50**, 1675 (1994).
[15] M. P. van Exter, G. Nienhuis, and J. P. Woerdman, Phys. Rev. A **54**, 3553 (1996).
[16] L. A. Coldren and S. W. Corzine, *Diode Lasers and Photonic Integrated Circuits* (Wiley, New York, 1995).
[17] G. Björk, A. Karlsson, and Y. Yamamoto, Appl. Phys. Lett. **60**, 304 (1992).
[18] R. Jin *et al.*, Phys. Rev. A **49**, 4038 (1994).
[19] Y.-S. Choi *et al.*, Phys. Rev. http://arxiv.org/abs/physics/0601190 (to be published).
[20] D. Bimberg *et al.*, IEEE J. Sel. Top. Quantum Electron. **3**, 196 (1997).
[21] J. Vuckovic, O. Painter, Y. Xu, A. Yariv, and A. Scherer, IEEE J. Quantum Electron. **35**, 1168 (1999).
[22] A. Badolato *et al.*, Science **308**, 1158 (2005).
[23] K. Hennessy *et al.*, Appl. Phys. Lett. **87**, 021108 (2005).
[24] R. J. Warburton *et al.*, Nature (London) **405**, 926 (2000).
[25] E. Moreau *et al.*, Phys. Rev. Lett. **87**, 183601 (2001).
[26] L. Besombes, K. Kheng, L. Marsal, and H. Mariette, Phys. Rev. B **63**, 155307 (2001); E. A. Muljarov and R. Zimmermann, Phys. Rev. Lett. **93**, 237401 (2004).
[27] M. Bayer, O. Stern, P. Hawrylak, S. Fafard, and A. Forchel, Nature (London) **405**, 923 (2000).